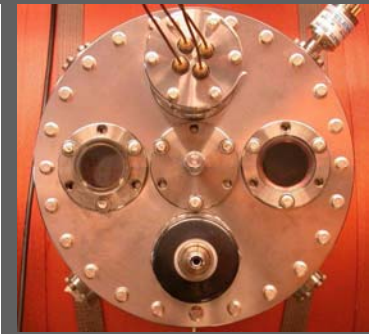
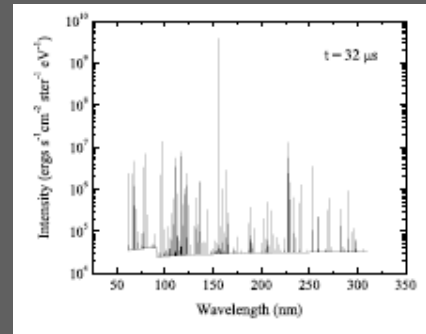
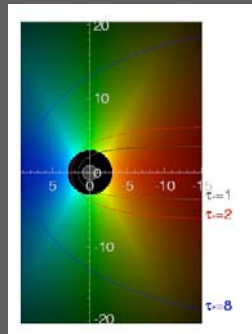
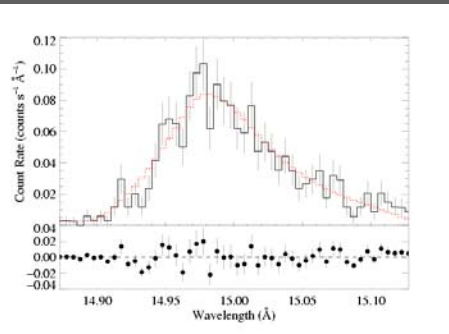
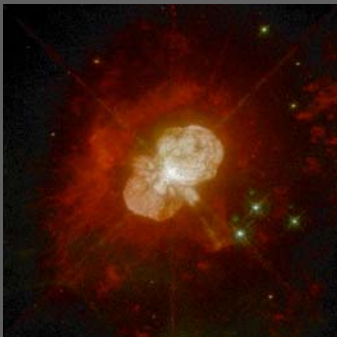


# Astrophysics Research Projects:

massive star winds, x-ray emission, theoretical models, spectroscopy, laboratory plasma astrophysics

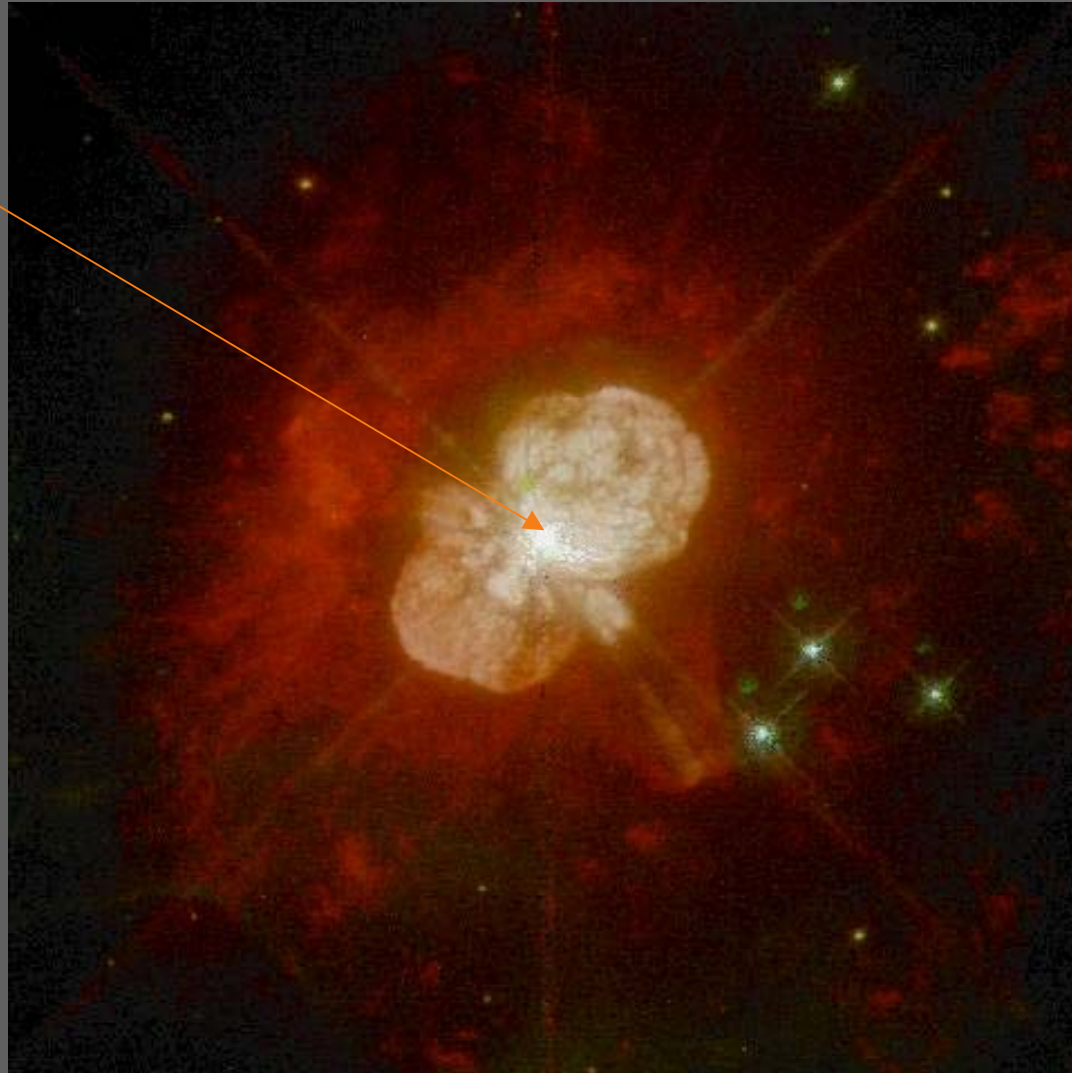
David Cohen

on leave 2007-08...but projects for the next few years



The most massive, luminous stars in the galaxy...

eta Carina

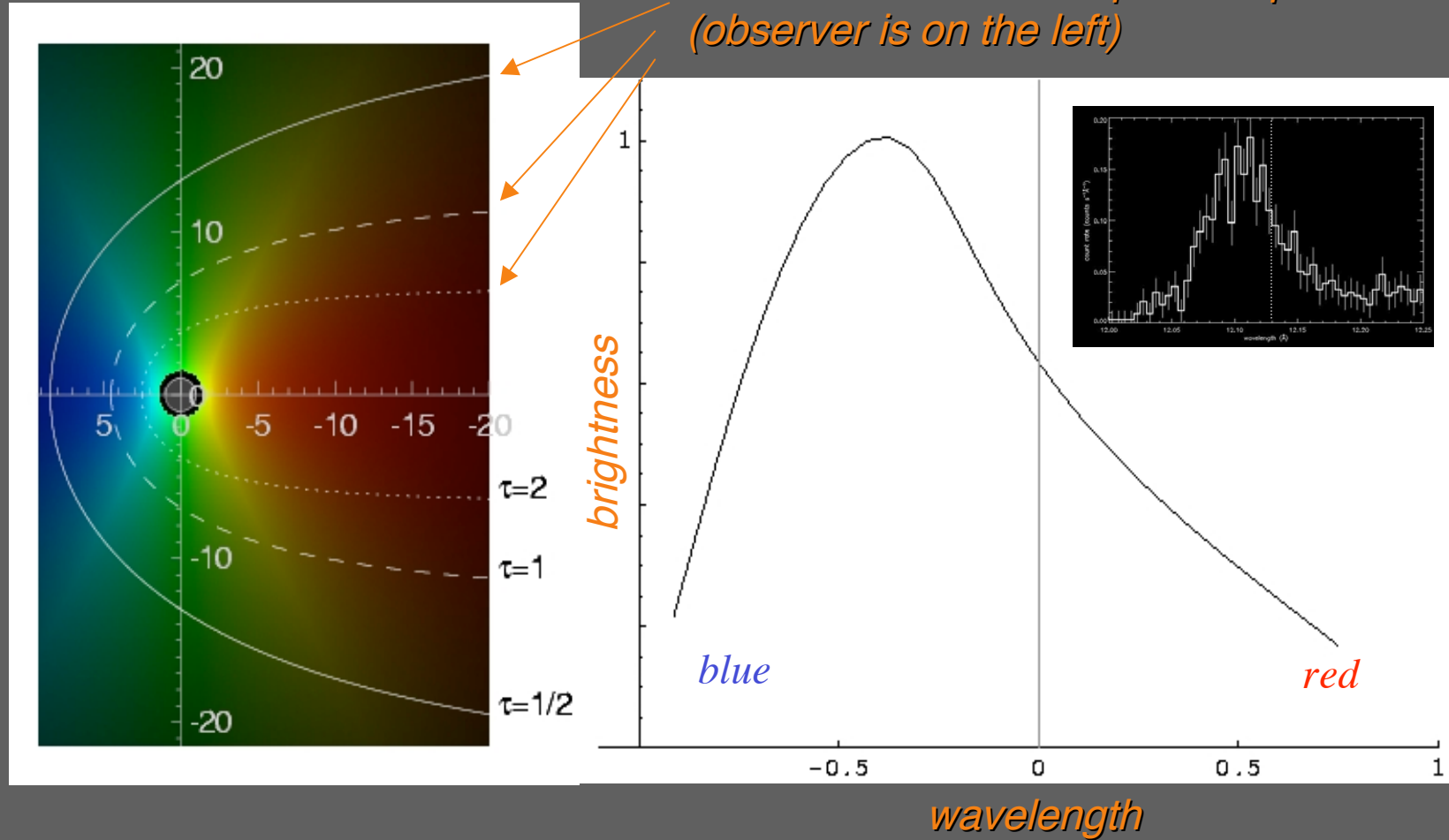


...have powerful radiation-driven **stellar winds**.

The *Chandra X-ray Observatory* (artist's conception)



*Contours of constant optical depth  
(observer is on the left)*



Model of wind x-ray emission and absorption (visualization: left;  
resultant X-ray emission line profile: right; data: inset)

# The basic wind-profile model

key parameters:  $R_o$  &  $\tau_*$

$$j \sim \rho^2 \text{ for } r/R_* > R_o, \\ = 0 \text{ otherwise}$$

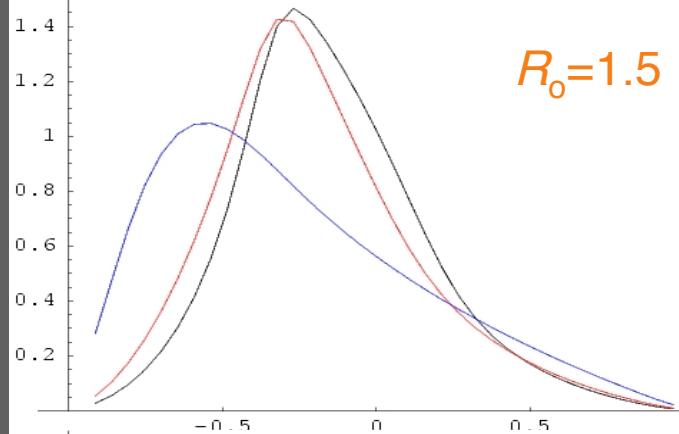
$$\tau = \tau_* \int_z^\infty \frac{R_* dz'}{r'^2 (1 - R_*/r')^\beta}$$

$$\tau_* \equiv \frac{\kappa \dot{M}}{4\pi R_* v_\infty}$$

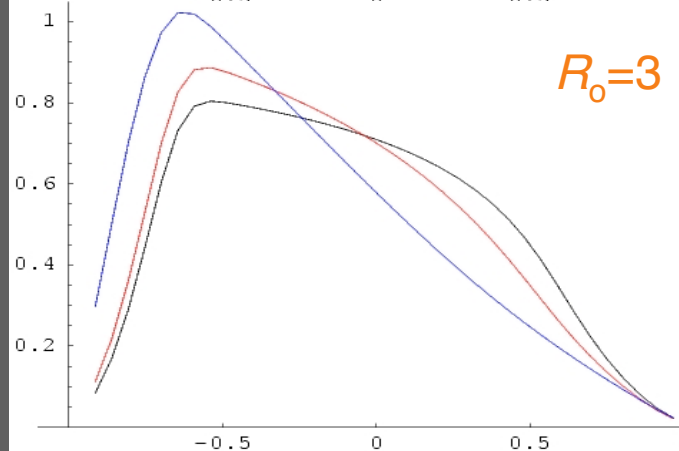
- Adjust the model parameters
- Fit the data
- Derive the physical properties of the wind from the x-ray line profiles

$\tau_* = 1, 2, 8$

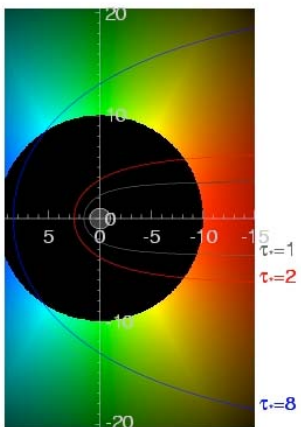
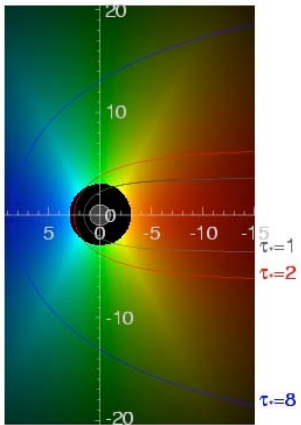
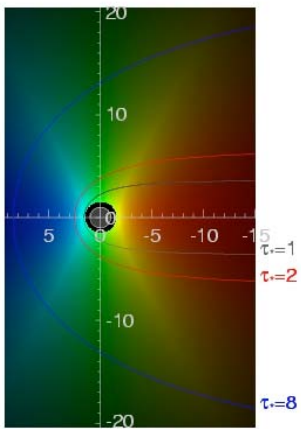
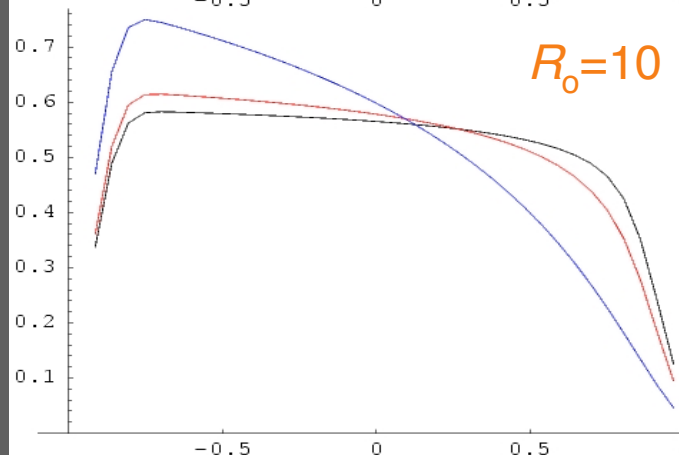
$R_o = 1.5$



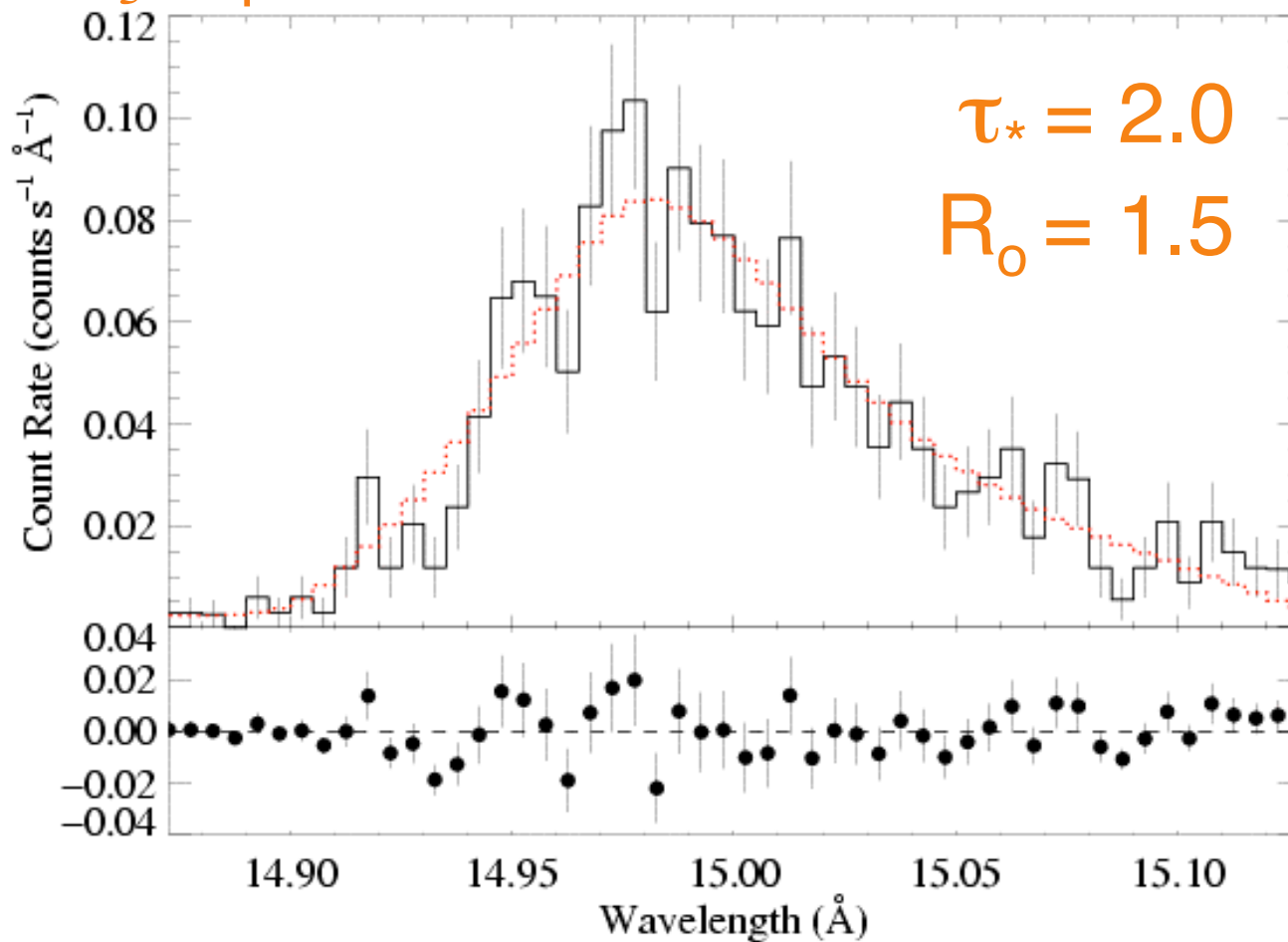
$R_o = 3$



$R_o = 10$



## $\zeta$ Pup: Fe XVII line at 15.014 Å - *Chandra*

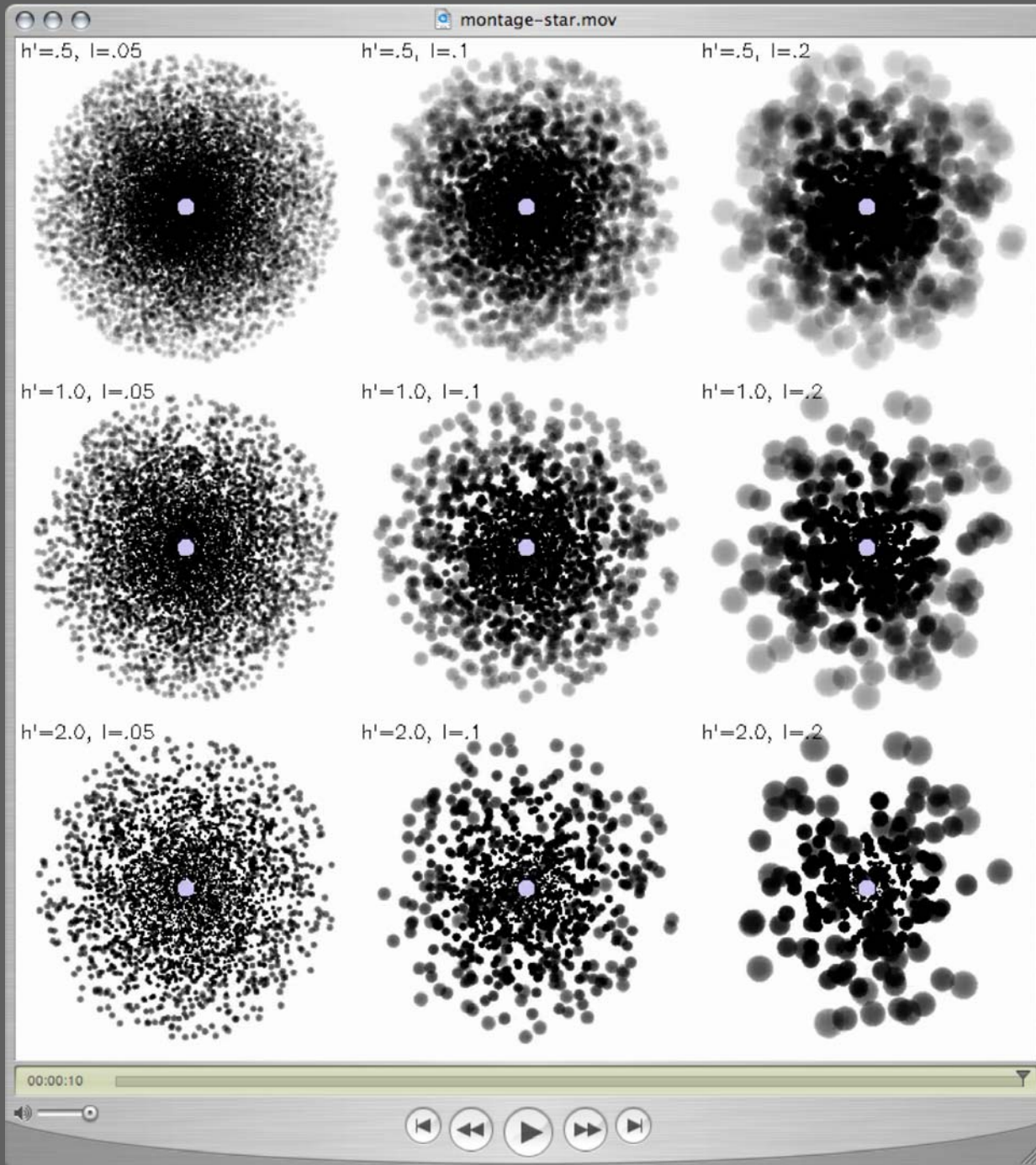


Major science result: less absorption than expected - stellar wind mass-loss rates have been overestimated (Roban Kramer, '03); Kramer, Cohen, & Owocki, *Ap.J.*, 592, 532; Cohen et al., *MNRAS*, 368, 1905.

Could **clumping** in the stellar wind play a role?

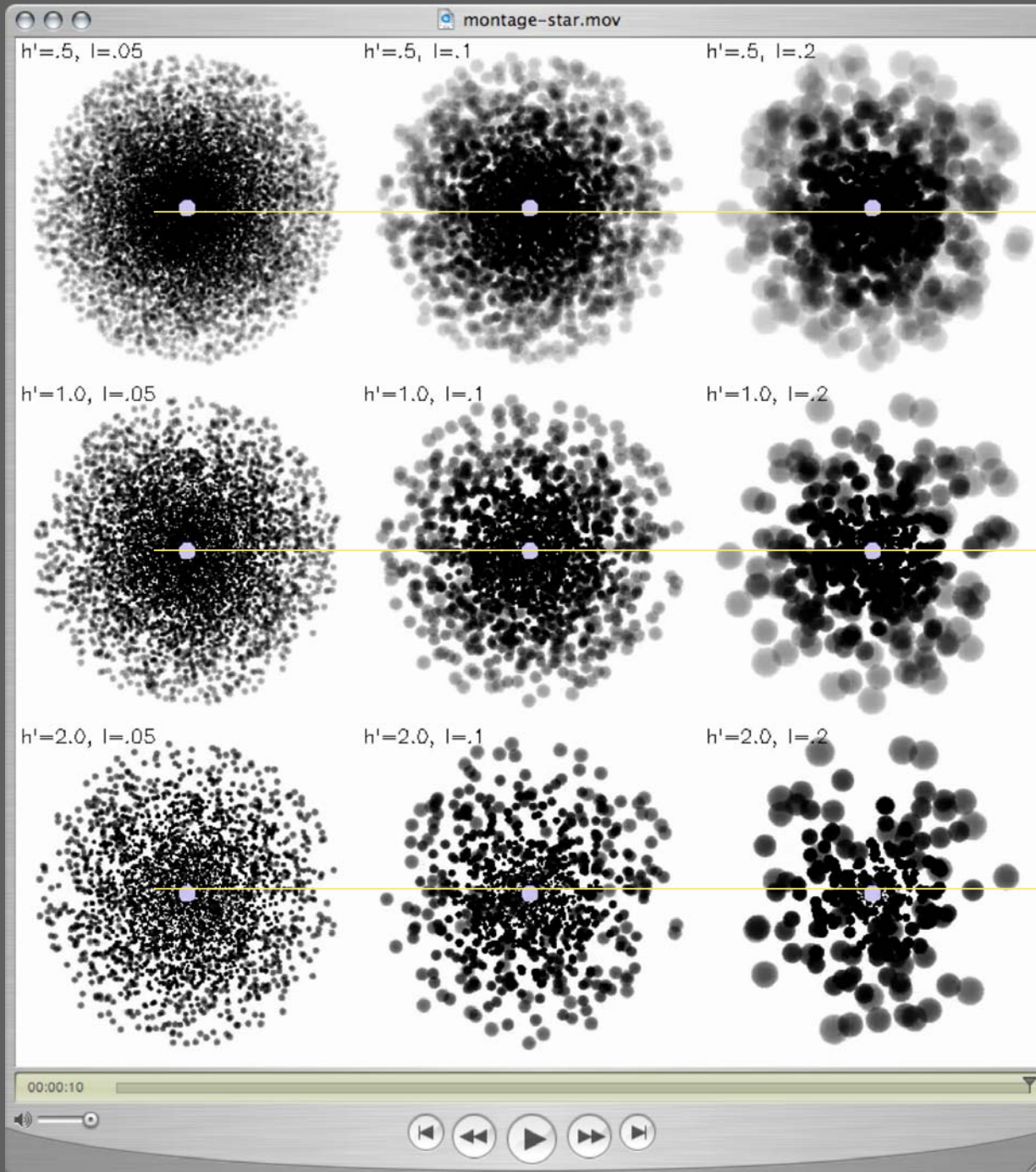
We've been making theoretical models of wind clumping and analyzing its effect on x-ray line profiles.

Owocki & Cohen, *Ap.J.*, 648, 565



$$h = (L^3 / \ell^2) = \ell / f$$

where  $h$ , the 'porosity length' is the key parameter;  $\ell$  is the clump size and  $f$  is the volume fraction filled by clumps



$$h = h'r$$

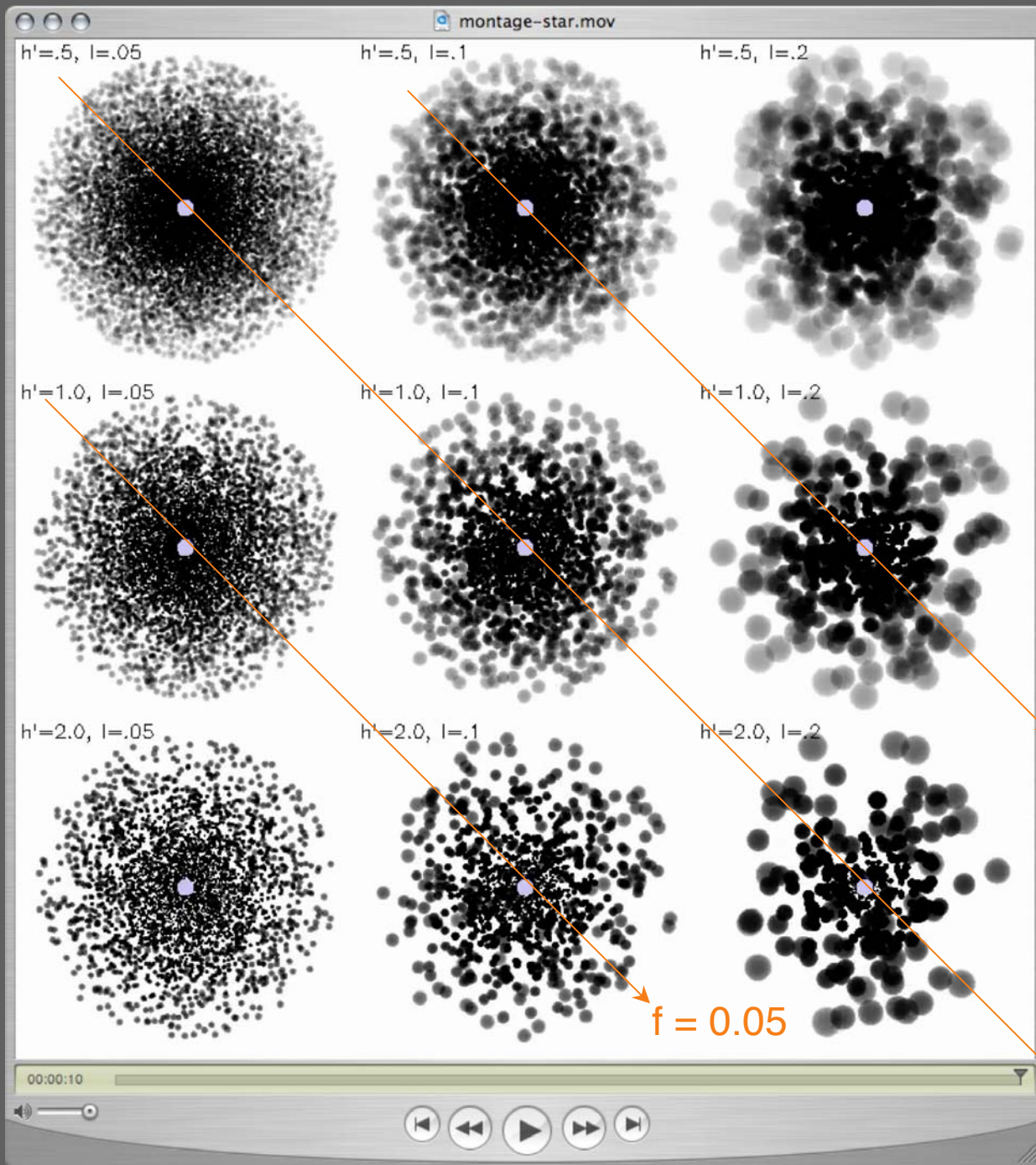
$$h' = 0.5$$

$$h = (L^3 / \ell^2) = \ell / f$$

$$h' = 1.0$$

$$h' = 2.0$$

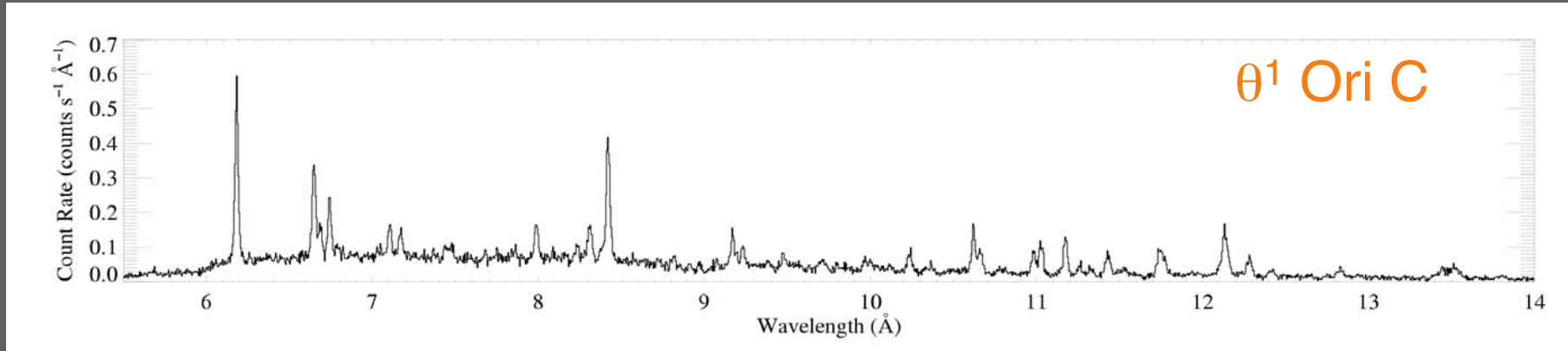
Models in the same row have the same effect on x-ray line profiles.



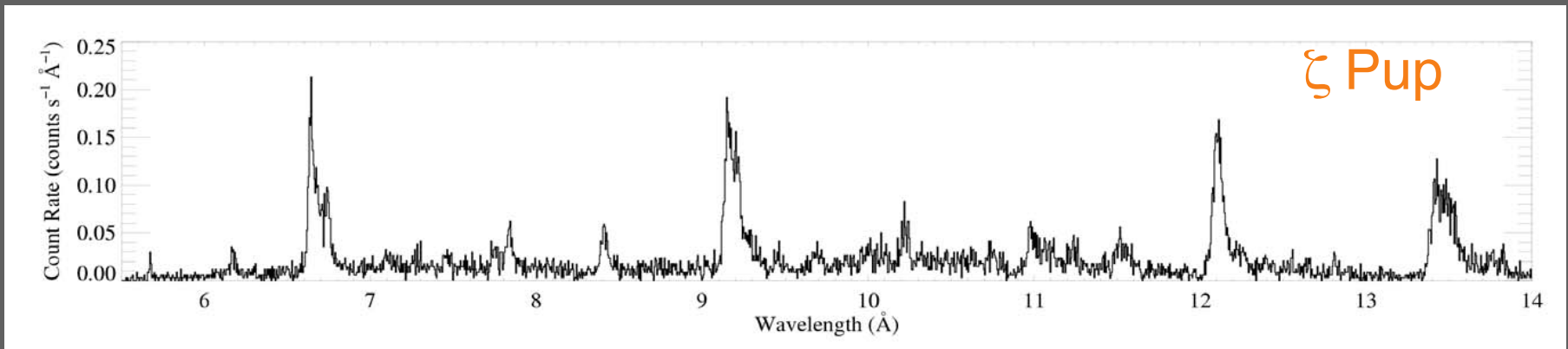
Models on the same diagonal have the same effect on other mass-loss diagnostics.

$$h = (L^3 / \ell^2) = \ell / f$$

## Chandra spectra of massive stars: survey of trends



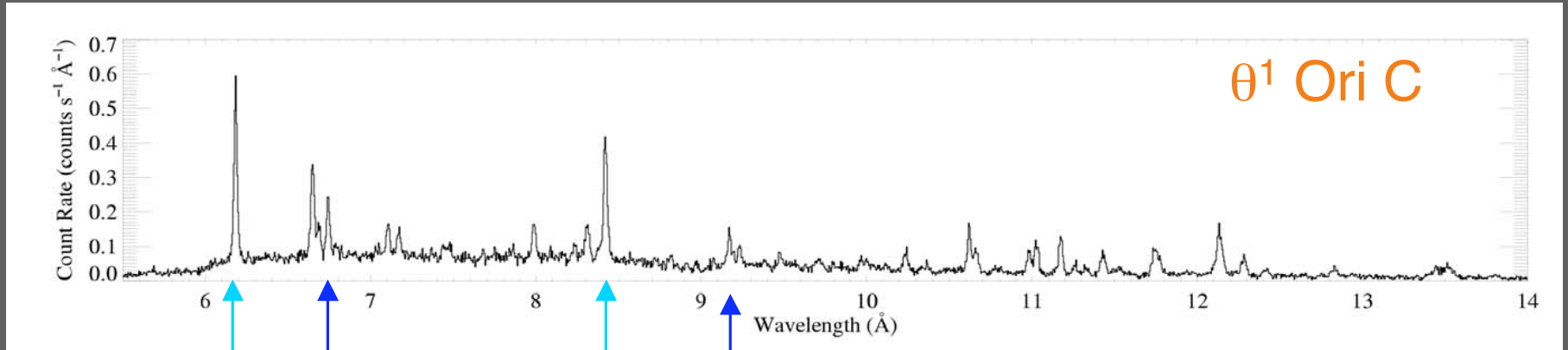
$\theta^1$  Ori C: hotter plasma, narrower emission lines



$\zeta$  Pup (O4 I): cooler plasma, broad emission lines

Cohen, *IAU Symposium 250*, Cambridge Univ. Press, 2008

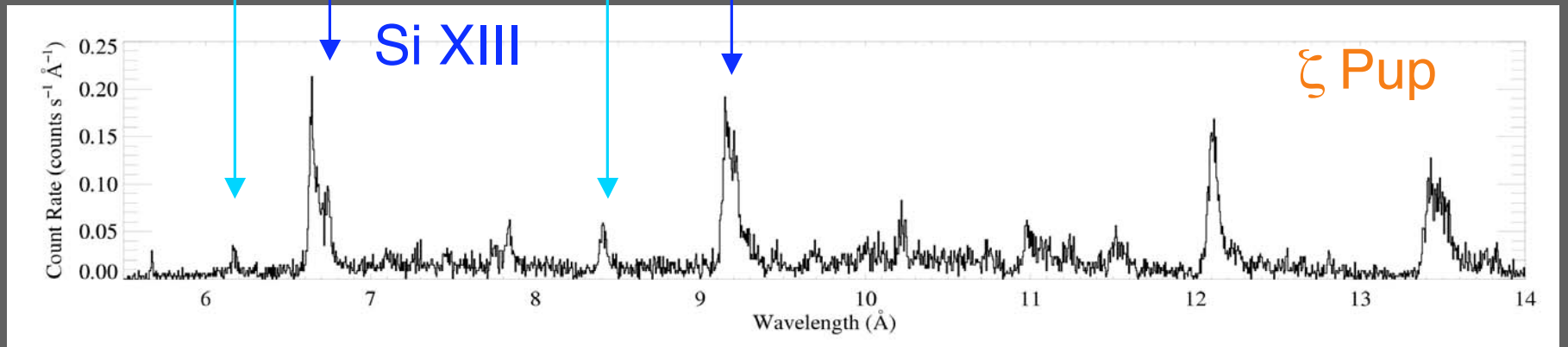
# H-like/He-like ratio is temperature sensitive



Si XIV

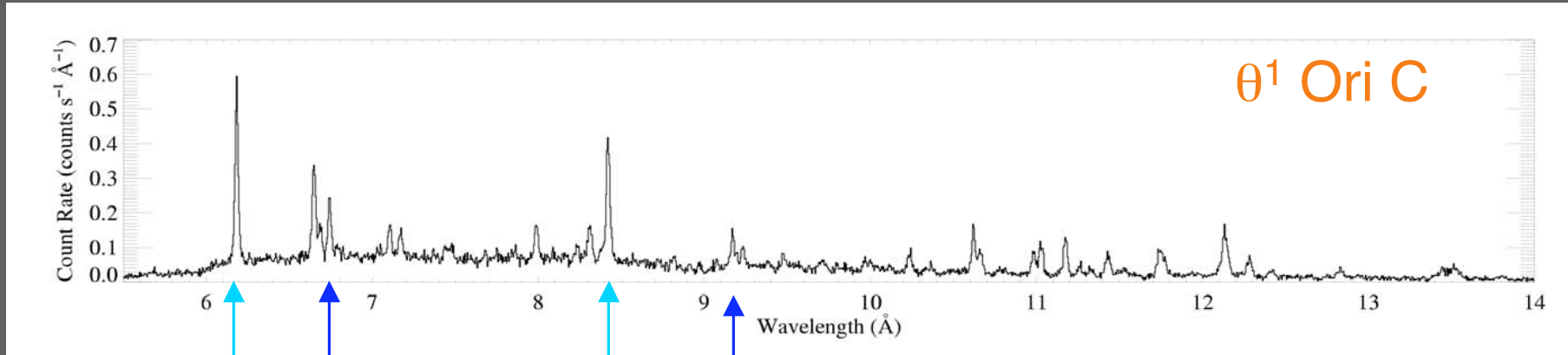
Mg XII

Mg XI



Si XIII

# The young O star – $\theta^1$ Ori C – is hotter



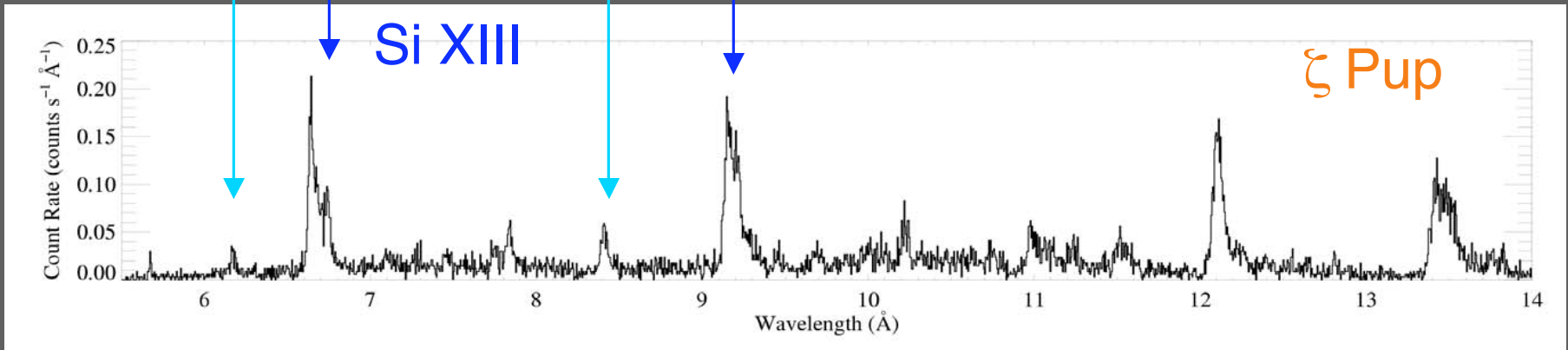
Si XIV

Mg XII

Mg XI

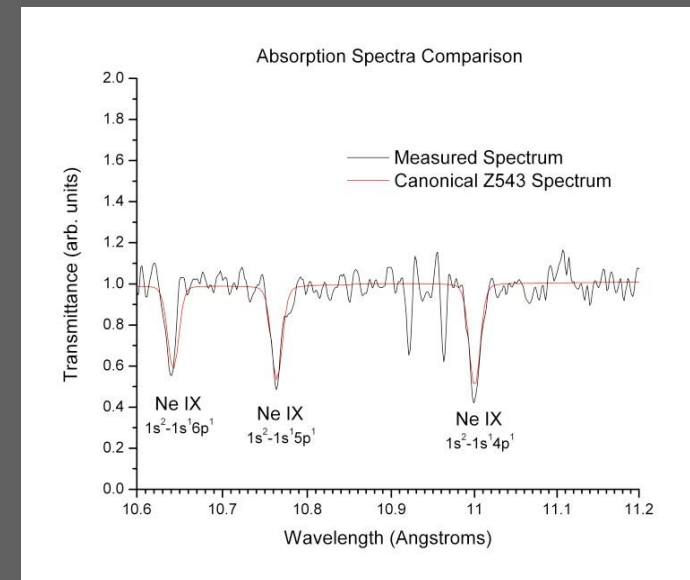
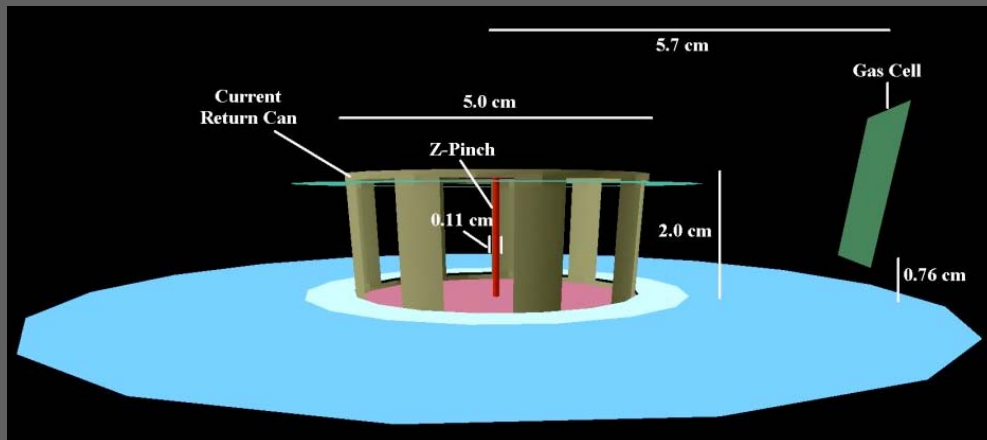
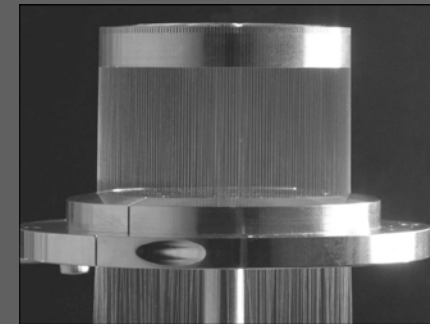
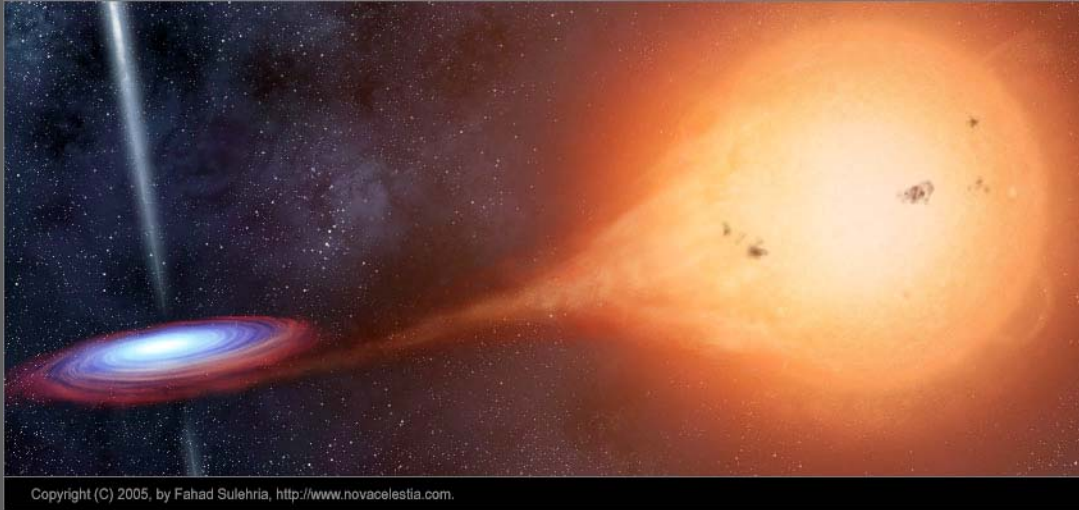
Si XIII

$\zeta$  Pup



# Laboratory Astrophysics

# Creating an X-ray photoionized nebula in the laboratory: Imploding wire array experiments on the Z-machine at Sandia National Laboratory



Mike Rosenberg's ('08) honors thesis

# Swarthmore Spheromak Experiment: magnetic reconnection in solar and space plasmas

Using x-ray and UV spectroscopy to diagnose  
the plasma temperature and kinematics

## Temperature and Flow Measurements During Magnetic Reconnection at SSX

Vernon H. Chaplin, Jason Horwitz, Michael R. Brown, and David H. Cohen  
*Department of Physics and Astronomy, Swarthmore College, Swarthmore, Pennsylvania 19081*

Chris D. Cothran  
*Department of Physics and Astronomy, Swarthmore College, Swarthmore, Pennsylvania 19081 and  
Department of Physics and Astronomy, Haverford College, Haverford, Pennsylvania 19041*

Temperature and flow measurements during counter-helicity spheromak merging studies at the Swarthmore Spheromak Experiment (SSX) [M. R. Brown, *Phys. Plasmas* **6**, 1717 (1999)] are presented. Low-resolution spectroscopy using a four-filter soft x-ray detector (SXR) is supplemented by VUV monochromator measurements of impurity emission lines. Comparison of these data with model spectra produced by the non-LTE excitation kinematics code PrISM SPECT [reference for PrISM SPECT] yields the electron temperature in the plasma with  $1 \mu\text{s}$  time resolution. C III temperature, measured with an ion Doppler spectrometer (IDS) [C. D. Cothran *et al.*, *Rev. Sci. Instrum.* **77**, 063504 (2006)] is seen to increase from 20-30 eV to 80-100 eV during spheromak merging. However, evidence for electron heating during magnetic reconnection is minimal: SXR and VUV line ratio measurements both yield  $T_e \approx 30$  eV on average. Mach probe measurements imply azimuthal bulk plasma flow velocities reaching 10 km/s during reconnection, confirming the presence of bidirectional jets as detected previously by IDS [M. R. Brown *et al.*, *Phys. Plasmas* **13**, 056503 (2006)]. The VUV emission line measurements are also used to constrain the concentrations of various impurities in the SSX plasma, which appear to be dominated by carbon.

### I. INTRODUCTION

Magnetic reconnection is the process driving the dynamics in spheromak merging and relaxation [1] as well as in several astrophysical scenarios [2]. During reconnection, magnetic energy is rapidly converted to electron and ion heat, plasma flow, and energetic particle beams [3, 4]. However, the partitioning of energy among various channels is not fully understood. Spheromak dynamics have been studied at the Swarthmore Spheromak Experiment (SSX) in a number of geometries [2, 5–8]. We have recently been studying spheromak merging in a prolate 0.4 m diameter, 0.6 m length, 3 mm wall copper flux conserver at SSX (see Figure 1). In these experiments, merging of a pair of counter-helicity spheromaks generates magnetic reconnection dynamics near the midplane.

Local and global magnetic structure of SSX spheromaks has been studied with up to 600 individual internal magnetic probes operated simultaneously at 1.25 MHz using a multiplexer system [9]. Line averaged electron density is monitored with a quadrature HeNe

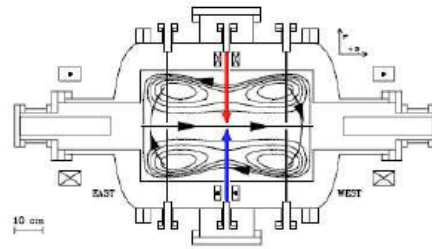


FIG. 1: Schematic of SSX. A cross-section is shown—the device is cylindrically symmetric about the horizontal axis in the figure. Spheromak plasmas are formed in the guns on the east and west sides of the vacuum chamber and ejected into the main flux conserver. The arrows represent the lines of sight of the VUV monochromator (red), and the soft x-ray detector and ion Doppler spectrometer (blue). Mach probe measurements are likewise made along the midplane. Arrays of magnetic probes are shown as black lines in the figure. The contours represent the magnetic field lines of an FRC, the plasma structure that forms when two counter-helicity spheromaks merge. Figure modified from [6].

laser interferometer [3]. We can scan density in a range  $n_e = 1 - 10 \times 10^{14} \text{ cm}^{-3}$ , and find a typical value of  $5 \times 10^{14} \text{ cm}^{-3}$ . SSX plasmas have temperatures  $T_e \leq T_i \approx 80$  eV, and typical magnetic fields of 0.1 T. The plasma is fully ionized and fully magnetized, with the ion gyroradius,  $\rho_i \ll R$ , where  $R = 0.2 - 0.25$  m is the outer flux conserving boundary of the plasma (defined by a cylindrical copper wall). The Lundquist number  $S$ , the ratio of the resistive magnetic diffusion time  $\tau_R$  to the Alfvén transit time  $\tau_A$ , is large for SSX,  $S \approx 1000$ . Accordingly, the global structure of SSX spheromaks is fully in the magnetohydrodynamic (MHD) regime ( $S \gg 1, \rho_i \ll R$ ).

Because magnetic reconnection is dynamically three-dimensional, it is often difficult to experimentally or observationally identify the reconnection site within the experimental volume or to determine whether the reconnection process has convected into the line of sight. In the experiments reported here, spectroscopic data are line-integrated over a 1 cm wide chord through a diameter at the midplane for about  $1 \mu\text{s}$ . In addition, an ensemble of 20-30 discharges are typically averaged for each

Vernon Chaplin's  
(‘07) honors  
thesis...and  
*Physics of Plasmas*  
paper.

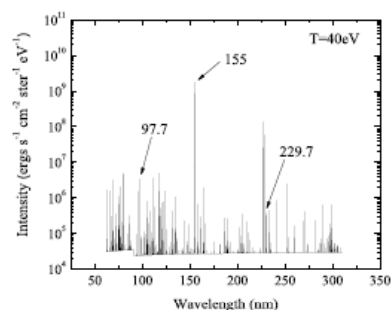
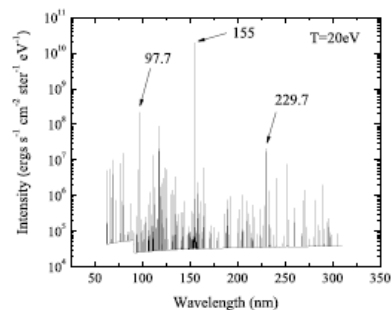


FIG. 3: Model spectra from steady-state simulations with  $T_e = 20$  eV (top) and  $T_e = 40$  eV (bottom). Both simulations assume a uniform 40 cm thick plasma composed of 99% hydrogen and 1% carbon with an ion density of  $5 \times 10^{14} \text{ cm}^{-3}$ . The temperature dependence of the  $I_{97.7}/I_{155}$  line ratio is evident, as is the weakness of the C III 229.7 nm line in the model spectra (which we discuss in section VI) relative to the other carbon lines. Note also the presence of the Lyman edge at 91.2 nm, indicating that radiative recombination of hydrogen rather than bremsstrahlung is the dominant continuum process at work.

### III. IMPURITY DETERMINATIONS FROM VUV LINE MEASUREMENTS

Individual emission line strengths are measured in SSX using a vacuum ultraviolet (VUV) monochromator with a focal length of 0.2 m. Photons enter the device through a slit of adjustable width and strike a selective diffraction grating, which selects and refocuses a narrow bandwidth around the desired central wavelength. Light leaving the diffraction grating is directed through an exit slit of adjustable width and into an 800 V photomultiplier tube (PMT). 500  $\mu\text{m}$  was found to be the optimal exit slit width, corresponding to a spectral resolution of 2 nm.

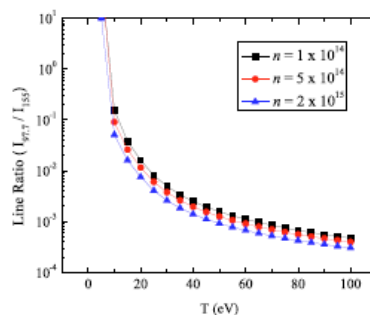


FIG. 4: Simulated  $I_{97.7}/I_{155}$  line ratio plotted as a function of temperature for three different plasma densities. Note the mild density dependence of this line ratio.

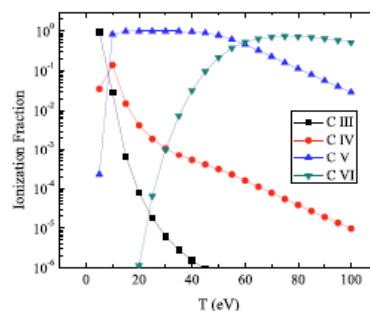


FIG. 5: Carbon ionization balance vs. electron temperature for an electron density of  $5 \times 10^{14} \text{ cm}^{-3}$ .

Signals from the PMT pass through a Stanford Research Systems SR570 current amplifier and are registered at 10 ns intervals by an oscilloscope and transferred to a computer using LabView.

A wavelength calibration curve for the monochromator was constructed by finding the wavelength of peak intensity of a number of impurity lines known to be visible in the SSX plasma (for example, lines that had been observed with ion Doppler spectroscopy). However, intensity calibration using a known plasma source has not been carried out. By slowly scanning across the wavelengths around each line, we have ensured that lines are correctly identified and that measurements are made at the line centers, but the possibility exists that a wavelength dependence in the monochromator's intensity cal-

We calculate model UV/x-ray spectra and compare them to the data collected with various spectrometers in the SSX lab

Theoretical modeling: computers, white board

Data (mostly high-energy spectroscopy): from space;  
from the SSX lab (and the Z-machine at Sandia)

By next year... optical spectroscopy with  
our new 24-inch telescope on the roof of  
the Science Center











This could  
be you in  
summer  
2009...but  
maybe  
without the  
flannel shirt.

